ANNUAL REVIEWS

Annual Review of Control, Robotics, and Autonomous Systems

Exploiting Liquid Surface Tension in Microrobotics

Antoine Barbot,[1] Francisco Ortiz,[1] Aude Bolopion,[1] Michaël Gauthier,[1] and Pierre Lambert[2]

[1]FEMTO-ST Institute, CNRS UMR 6174, Université Bourgogne Franche-Comté, Besançon, France; email: antoine.barbot@femto-st.fr

[2]Transfers, Interfaces, and Processes (TIPs), Université Libre de Bruxelles, Brussels, Belgium; email: pierre.lambert@ulb.be

Annu. Rev. Control Robot. Auton. Syst. 2023. 6:313–34

First published as a Review in Advance on November 30, 2022

The *Annual Review of Control, Robotics, and Autonomous Systems* is online at control.annualreviews.org

https://doi.org/10.1146/annurev-control-062422-102559

Keywords

surface tension, capillary forces, microrobotics, micromanipulations

Abstract

Surface tension effects are known to be dominant at the submillimeter scale. Within this context, the literature has extensively described the underlying physics (e.g., surface tension, wetting, surface texturation, and coatings), and capillary forces have been exploited in a variety of applications (e.g., capillary picking, self-alignment, capillary sealing, and capillary bearings). As several stimuli can be used to control liquid menisci, these forces have been used mainly in microrobotics in open loop (i.e., without real-time feedback). However, at least two major sources of uncertainty hinder these forces from working properly in open loop: the variability due to contact-angle hysteresis (the difference between wetting and unwetting) and the variability in the involved volume of liquid. To be able to reject these disturbances, successful sensor integration and associated advanced control schemes need to be embedded in capillary microrobotic microsystems. This article analyzes research contributions in this field from three different perspectives: the stimulus action of the surface tension effect (light, B-field, etc.), the application field (actuation, picking, sealing, etc.), and the sensing and control schemes. Technologically complex developments coexist with elegant and straightforward engineering solutions. Biological aspects of surface tension are not included in this review.

1. INTRODUCTION

Surface tension effects have probably been known since the early days of humankind, from observing water striders on the free surfaces of rivers to using natural sponges to carry liquid. Surface tension has been scientifically reported since at least the eighteenth century, with the contribution of James Jurin on capillary rise (1). Until the end of the twentieth century, most of the scientific research on capillarity was limited to equilibrium situations (Laplace) or escapes out of the equilibrium, namely instabilities (Rayleigh, Plateau, etc.). In Section 2.1, we briefly discuss these historical contributions and the current understanding of surface tension effects. Physicists have identified parameters that drive capillarity, meniscus and droplet shapes, and the consequent capillary forces (e.g., surface tension and contact angles; see **Figure 1**), and engineers have identified stimuli that act on these parameters (discussed in Section 2.2), paving the way for a wide range of case studies, such as grippers, actuators, sealing, and fluid lenses.

Section 3 deals with modeling and controlling surface tension effects. It includes a detailed analysis of an effector sandwiched between a passive guiding meniscus and an active actuating meniscus. We also present a nondimensional analysis based on the so-called capillary number (*Ca*, the ratio of viscosity to surface tension) and Weber number (*We*, the ratio of inertia to surface tension) to assess whether static modeling is sufficient or more complex dynamic modeling must be considered. This map also makes it possible to compare works with different liquids and interfaces.

Section 4 provides an extensive description of applications of the meniscus to microrobotics, which are also sorted in a nondimensional *We–Ca* map in Section 3.3 (**Figure 6**). From the point of view of a control engineer, most of these applications are still limited to passive applications of the surface energy minimization, without any external control (such as self-alignment), or they can, to a lesser extent, be considered actuators controlled in open loop (fluid lenses and capillary motors).

The research assumption leading to this review is that introducing more advanced control in surface tension–based applications can pave the way for a new field of research in microrobotics, namely wet or capillary microrobotics. Considering closed-loop control will enable two decisive advantages with respect to open-loop applications. First, it enables compensation for liquid evaporation, which results in a mostly unknown volume of liquid (water and other solvents evaporate

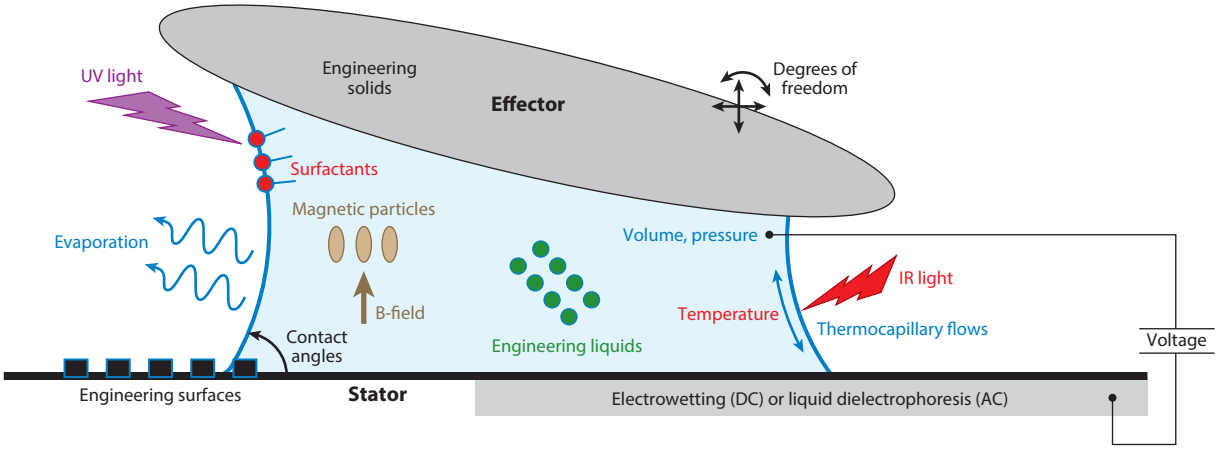

Figure 1

A capillary bridge at a dimension below the capillary length (2.7 mm for water), showing stimuli that can actuate a meniscus and a floating object acting as a microrobotic effector.

quickly at the submillimeter scale). Second, it enables control over the so-called contact-angle hysteresis (the difference between wetting and unwetting), which is rarely negligible, and uncertainty in the contact angle leads to a wide scattering in the value of the capillary forces. Engineering of surface geometry and chemistry is also critical for capillary mechanisms and can lead to elegant mechanisms such as fluidic valves and control of the wetting direction, which depends on the liquid surface energy (2). However, we chose to omit this aspect from our review, focusing instead on the active control of the interface.

The purpose of this review is to provide a more comprehensive view of all possible stimuli (control parameters) that can act on the underlying capillarity parameters and to capture the intimate interactions between input and output candidate parameters through models. Because closed-loop control can be envisaged only when the system state can be measured or estimated in real time, we also provide a list of proven sensing solutions. Considering the limitations of the current state of the art, these solutions have naturally not been integrated into full closed-loop control of capillary microsystems; overcoming this challenge will be an important goal for the future. Such wet or capillary microrobots would be interesting for many reasons: the scaling law, which implies a large capillary force at a small scale; the compliance and large displacements offered by interface deformation; integration in compact systems, such as fibers, while having important degrees of freedom; and simplicity of fabrication, as a single fluid joint can potentially combine actuation, mechanical joints, and manipulation of the environment.

2. THE PHYSICS OF THE MENISCUS AND CONTROL VARIABLES USABLE IN ROBOTICS

2.1. Basic Ingredients and Historical Note

This section is relatively brief, and we invite readers seeking more detail to consult the abundant literature on capillarity and surface tension. Historical texts include works on capillary rise by Jurin (1), on capillary pressure by Laplace (3), on the shapes of drops by Plateau (4), on the fundamentals of wetting by Wenzel (5), on the dynamics of flows by Washburn (6), and on the hydrodynamics of wetting by Tanner (7). Classical textbooks have been published by Adamson & Gast (8), Israelachvili (9), and de Gennes et al. (10).

The dominance of surface tension effects at scales smaller than a few millimeters enables "engineering below the capillary length" [as coined by Lambert (11)]. This capillary length is defined as the size at which surface tension and gravity effects balance one another:

$$L_C = \sqrt{\frac{\gamma}{\rho g}}, \qquad 1.$$

where γ is the surface tension (in N m^{-1}) of the considered liquid (e.g., water, oil, or liquid metal), ρ is its density, and g is 9.81 m s^{-2}. The effects of gravity can be neglected for systems with dimension largely lower than L_C, which for water is approximately 2.71 mm. More precisely, at equilibrium, L_C is the typical length scale at which the hydrostatic pressure $\rho g L_C$ generated in a meniscus of height L_C would be exactly balanced by the so-called Laplace pressure generated by the surface tension and a meniscus curvature equal to L_C^{-1}.

Combined with the wettability of surfaces, the interplay between surface tension and gravity defines the geometrical shape of a meniscus. Mathematically, this shape is defined through its curvature $2H$, thanks to the so-called Laplace law:

$$2H = \frac{p_{in} - p_{out}}{\gamma}, \qquad 2.$$

where $p_{in} - p_{out}$ is the pressure gap across the interface due to surface tension. Wetting conditions are seen as the boundary conditions of this problem. The shape of the meniscus defines the amount of force exerted by the meniscus on the surfaces enclosing it. There are two contributors to this force (12): the pressure force arising from the Laplace pressure gap, called the capillary, pressure, or Laplace force, and the resulting tensile action of the liquid–air interface on the solids along the triple line (the line intersecting the liquid, the air, and the solid), called the tensile or tension force. The so-called capillary forces are the combination of these two forces. Let us note that the problem can also be described in terms of minimizing surface energy (in addition to the textbooks already mentioned, see Reference 13).

Finally, it is important to consider that the surface energy between the solid and the liquid (as well as between the solid and the gas) plays a crucial role when engineering a system below the capillary length. This directly impacts the contact angle of a liquid meniscus (defined by the angle between the solid–liquid and liquid–gas interface on a plane surface) as described by the Young equation:

$$\cos\theta = \frac{\gamma_{sg} - \gamma_{sl}}{\gamma_{lg}}, \qquad 3.$$

where θ is the contact angle and γ_{sg}, γ_{sl}, and γ_{lg} are the surface energy between the solid and the gas, the solid and the liquid, and the liquid and the gas, respectively. For $\theta < 90°$, the surface is said to be hydrophilic, and for $\theta > 90°$, the surface is said to be hydrophobic.

Surface roughness tends to render hydrophilic surfaces more hydrophilic (lowering their apparent contact angle) and hydrophobic surfaces more hydrophobic (increasing the apparent contact angle), an effect that is described by the Wenzel model as long as air is not trapped in the vicinity of the solid–liquid interface. Air can become trapped at the interface on rough hydrophobic surfaces (often engineered to exhibit this feature), leading to a brutal increase of the apparent contact angle and thereby creating super-hydrophobic surfaces; in this case, the Cassie–Baxter model can be used.

A complete introduction to these subjects can be found in the textbook by de Gennes et al. (10; for wetting behavior, see section 1.2 of chapter 1, and for wetting of textured surfaces, see section 2 of chapter 9).

2.2. Stimuli to Act on a Fluid Meniscus

There are five principal means of deforming a liquid meniscus, resulting in a displacement and/or a force: controlling the pressure difference between the liquid and the environment, controlling the volume of the meniscus, generating a flow inside the meniscus, acting on the contact angle, and using a volume force on the fluid to change the shape of the meniscus. For each of these means, the literature provides a variety of stimuli (such as an electric field or light) for microroboticians to use as control parameters. Different actuation paths are possible; the primary ones are shown in **Figure 2**, and some examples discussed below are shown in **Figure 3**. The following describes each of these five means as well as the different paths linking the stimulus inputs to the final meniscus deformation. It also provides insight on the different advantages and drawbacks of each actuation path, particularly for microrobotic applications.

2.2.1. Controlling the pressure difference. The first means of deforming a liquid meniscus is to control the pressure difference between the liquid and the environment. This difference is directly linked to the curvature of the interface according to the Laplace law (Equation 2). A concrete example is detailed in Section 3 (Equations 4 and 5).

Pressure control allows good repeatability, particularly if the triple line of the meniscus remains pinned to the same location. Note that controlling meniscus geometry with pressure usually first

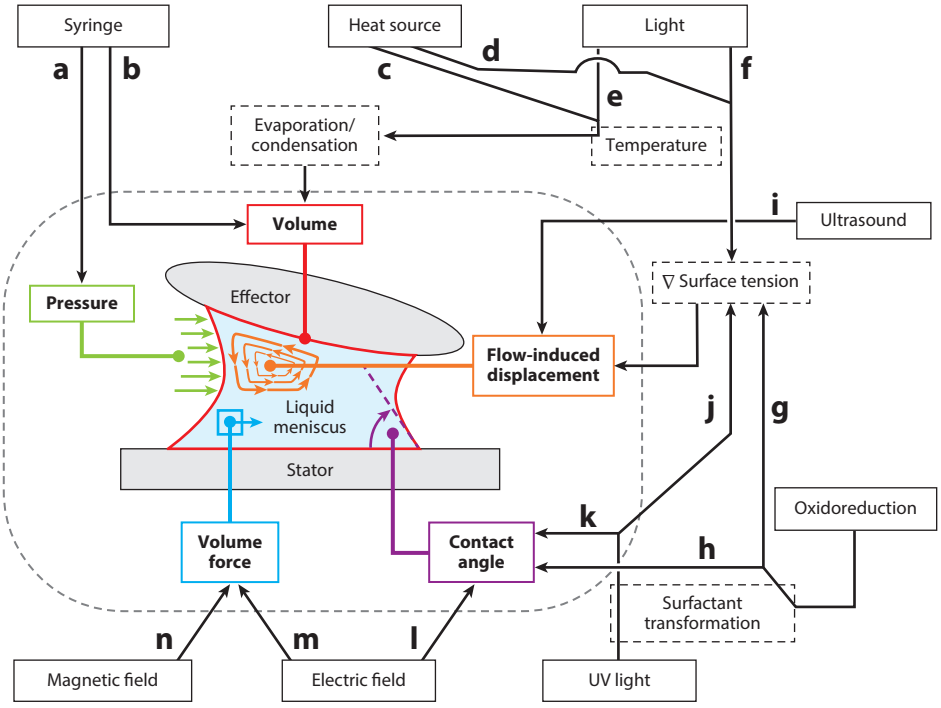

Figure 2

Classification of different means of actuating a liquid meniscus. (*a*) Direct pressure change (14, 15). (*b*) Direct volume change (16, 17). (*c*) Volume change through temperature-induced evaporation using a Peltier element (18). (*d*) Heat source–induced Marangoni flow (19, 20). (*e*) Light-induced evaporation (21). (*f*) Light-induced thermocapillary flow, either globally with broad light (22) or locally with a laser (23–25). (*g*) Oxidoreduction to create a surfactant gradient (26). (*h*) Oxidoreduction reaction on the surface to induce a change in contact angle (26, 27). (*i*) Ultrasound (28). (*j*) Use of a UV-reacting chemical to induce a surface tension gradient (29–31). (*k*) Use of a UV-reacting chemical to induce a change in contact angle (32, 33). (*l*) Electrowetting (34–37). (*m*) Dielectrophoretic manipulation (38–40), electromigration (41), or charge-induced deformation (42). (*n*) Magnetic field actuation (ferrofluid) (43–46).

presents a stable domain, where an increase of the pressure decreases the curvature. This domain is followed by an unstable one, where an increase of the pressure increases the curvature, which results in the leakage of the device by overflowing the meniscus. When the meniscus is used to seal a micropiston (14, 15) (**Figure 3*c***), this unstable domain corresponds to the pressure limit, resulting in a breach of the meniscus and loss of the seal (**Figure 2**, path *a*). Direct pressure through a syringe or pump-based controller benefits from relatively simple fabrication and integration (although it still requires a connection through a microchannel or capillary tube) with a connection to a fluid input linked to a pressure controller, which can even be manually controlled.

2.2.2. Controlling the volume of the meniscus. The second means is to control the volume of the meniscus (e.g., **Figure 3*d***). Controlling the volume with a syringe (**Figure 2**, path *b*) has the same fabrication constraints as controlling the pressure with a syringe; however, control of the precise volume of the meniscus is highly sensitive to mechanical perturbations on the fluidic connections as well as their stiffness. Therefore, guaranteeing a repeatable measure requires a specific setup (17) or direct visual feedback. Modeling of the force and displacement is also challenging, as the shape of the meniscus needs to be found by solving the minimal surface energy configuration

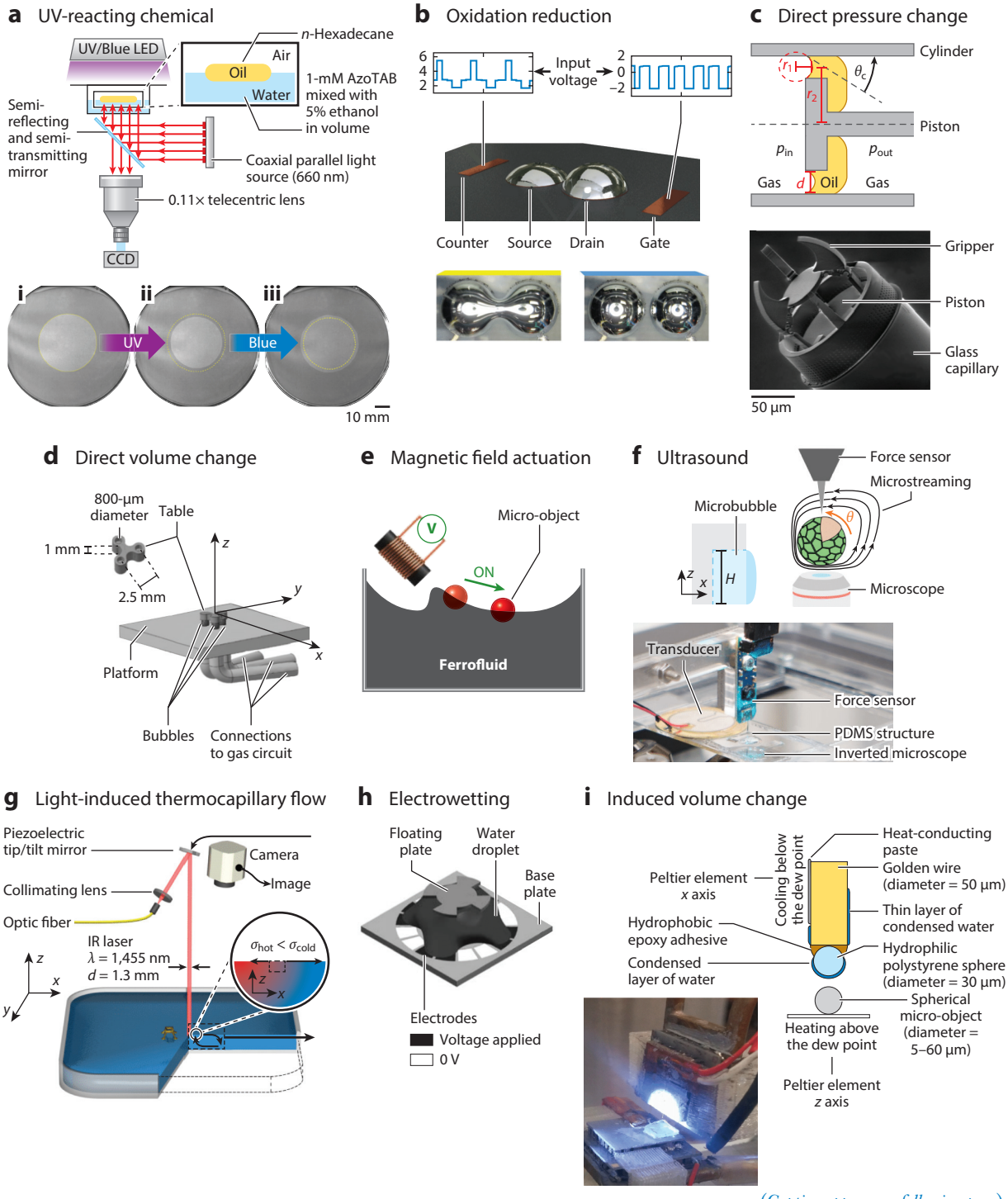

(*Caption appears on following page*)

Figure 3 (*Figure appears on preceding page*)

Examples of different means of actuating a liquid meniscus. Abbreviations: AzoTAB, azobenzene trimethylammonium bromide; PDMS, polydimethylsiloxane; V, voltage. Panels *a*, *d*, *e*, *g*, and *h* adapted with permission from References 32 (**https://pubs.acs.org/doi/10.1021/acsomega.9b03039**; further permissions related to material from this work should be directed to the American Chemical Society), 16, 43, 24, and 34, respectively; panels *b*, *c*, *f*, and *i* adapted from References 27, 15, 28, and 18, respectively (CC BY 4.0).

corresponding to a specific volume. However, volume control of the meniscus is possible in the unstable domain mentioned for pressure control. Pressure and volume control are linked and allow only 1D actuation per meniscus, as only one value can be set. Increasing the degrees of freedom requires using multiple menisci (16), which makes fabrication and integration more challenging, as the axis symmetry of the device is lost and merging of the different menisci needs to be prevented.

Volume can also be controlled through evaporation and condensation. These methods are usually used only as an on/off control, allowing the formation and suppression of a meniscus for gripping applications (the effector is then the object to grasp). Evaporation happens naturally, but heat can accelerate the process, and heat can be provided by an infrared laser (21) (**Figure 2**, path *d*). To increase the meniscus volume, it is also possible to use a cooling heat source (18) (**Figure 2**, path *c*; **Figure 3*i***). Electrical current can also be used to change the volume of a drop by taking advantage of an electromigration phenomenon in which mass transport occurs in the direction of the electron flux. To be nonnegligible, this phenomenon requires a high current density. Von Kleist-Retzow et al. (41) changed the volume of a conductive metal drop approximately 10 μm in size.

2.2.3. Generating a flow inside the meniscus. The third means is to generate a flow inside the meniscus to apply force and displacement on a floating effector through the resulting pressure field and viscous stress. The most common method to generate such a flow is to create a local surface tension gradient. This gradient induces a flow, called the Marangoni effect, which is set at the interface from an area of low surface tension to one of high surface tension. Temperature differences can be used to generate such a gradient (in which case the phenomenon is referred to as thermocapillary flow), as surface tension generally decreases with temperature in liquid. Such gradients can be directly generated on the surface in contact with the liquid (19, 20) (**Figure 2**, path *d*) or using light-induced heating (**Figure 2**, path *e*).

Broad light-induced heating of the overall meniscus (where the light shines through a microscope objective) with an asymmetric microscopic floating effector has been demonstrated to perform rotation at up to 300 rpm (22). Here, the intensity of the light was directly used to modulate the rotation speed path. However, integrating more degrees of freedom with this method seems challenging. Alternatively, the selective heating position point can be set by using a laser spot, which can allow 2D control of floating effectors in closed loop (24) (**Figure 3*g***), gas drops in liquid (stable control, where the drop moves to the laser position) (25), or particle displacement in plastic fiber (23). The intrinsic advantage of light actuation is that visual feedback is usually possible through the same optical path as the actuation, enabling one to position the heat source and manipulated object relative to one another without complex initial calibrations.

A chemical approach can also create a flow induced by a surfactant gradient. The simplest method is to add surfactants to a particular meniscus position. Centimeter-sized soap-propelled boats can be propelled this way, finding applications mainly as toys. Indeed, the motion stops after a few seconds when the Marangoni flow has homogenized the surfactant on the entire meniscus surface. Even if volatile surfactants can be used to sustain propulsion until the depletion of the surfactant reservoir (47), the irreversibility of this process makes it difficult to use for control. Another approach is to use a light-sensitive chemical reaction, which generates surfactants where

the light is shined (32) (**Figure 3*a***). As light can be easily focused, this method benefits from the same advantage as light-induced thermocapillary actuation (31). Moreover, some chemical reactions can be tuned in two directions by using different wavelengths, allowing stable position control of microliters of oil droplets floating on an aqueous solution (30) to generate a surface tension difference of approximately 1 mN m^{-1}.

Electrical potential on a set of electrodes can precisely control the fabrication and depletion of redox-active surfactants (26). The advantages of this method (**Figure 2**, path *h*) are the ease of integration thanks to the maturity of electrode fabrication and voltage control, the potentially large number of degrees of freedom (as many as there are electrodes), and the important difference in surface tension, with a reported maximum difference of up to 22 mN m^{-1} for voltage in the 1-V range. Modeling the resulting flow and effector movement from the electrodes' voltage distribution is challenging, however, as the chemical reaction, surfactant diffusion, and fluid flow should be part of the model. Redox-active surfactants can also be used to unwet a specific region covered with electrodes (26).

Acoustic waves (**Figure 2**, path *i*) can also generate vibrations on the meniscus interface that control a fluid flow and may induce meniscus motion (e.g., **Figure 3*f***). The major advantage of this method is that it provides a way of multiplexing with a single generator by using different resonant frequencies of the fluid interface. For a gas-based meniscus in a liquid environment, Qiu et al. (48) demonstrated the use of an ultrasound for microrobot propulsion with several degrees of freedom. For a liquid meniscus, surface acoustic waves (49) or simply vibrations (50) result in drop movements.

2.2.4. Acting on the contact angle. The fourth means is to act on the contact angle of the triple lines—or, in other words, to change the hydrophobicity of the surface. The most common technique is electrowetting (**Figure 2**, path *l*). By applying either a DC field with a conductive liquid to attract the charge to the electrodes (51) or an AC field with a dielectric liquid to attract liquid between two close electrodes (or interdigitated electrodes) (40), one can reduce the apparent contact angle and deform the overall meniscus (36). This requires thin-film fabrication resources, as a dielectric layer with a hydrophobic surface needs to be patterned on the electrodes with a typical thickness of 0.5 μm or less.

Electrowetting is quite well known for droplet displacement at a predefined location by attracting droplets to a specific electrode. Therefore, it has been proposed for a microconveyor system (37) as well as a compact linear and translation step motor with a discrete set of possible motions based on a large number of fluid menisci (35). It has also been proposed recently in a microfluidic chip for an addressable valve array (52). Such a discrete approach allows open-loop repeatable control despite the hysteresis faces of the contact line. To drastically reduce the hysteresis, another approach is to use a liquid-infused substrate (53). A rotating motor has also been proposed, with an effector placed on a single meniscus and deformed by several electrodes (34) (**Figure 3*b***).

Finally, a light-sensitive resistive nanometric layer has been proposed for controlling electrowetting with a light pattern (54, 55). As for redox-active chemical-based stimuli, electrowetting has the advantage of relying on electrodes that can be easily designed in large numbers and in various shapes, potentially enabling the creation of effectors with multiple degrees of freedom. However, modeling the relationship between the applied voltage and the effector position is not trivial and remains a challenge. The contact angle of drops can also be globally changed by using UV light to activate a light-sensitive surfactant either on the liquid (32) or on the solid surfaces (33) (**Figure 2**, path *k*). Finally, the oxidoreduction path (27) (**Figure 2**, path *g*) can also be used globally to change the contact angle of a drop (e.g., **Figure 3*b***).

2.2.5. Using a volume force. The fifth means is to use a volume force on all of the fluid to change the shape of the meniscus. This approach enables simple control, as the volume force can be controlled remotely using an external field (magnetic or electric). The main drawback for microrobotics use is linked to the scale effect on this actuation aim: The volume force has a cubic dependency with the size of the setup, and this force decreases rapidly when the scale is reduced.

The first way to apply a volume force to a droplet is to use ferromagnetic fluid and either a permanent magnet (45) or an electromagnet (43, 44) to locally attract the fluid path (**Figure 2**, path *n*; **Figure 3*e***). This makes these methods relatively easy to use in practice without requiring complex setup or fabrication since different ferrofluids are now commercially available at an affordable price (approximately €100 per liter). Another way to apply a volume force is to use an electric field to deform and break the droplet's path (**Figure 2**, path *m*). The physics of this phenomenon has been extensively researched for both perfectly insulated liquids and leaky dielectrics (for an introduction to this topic, see Reference 56) and is the basis for the electrospinning and electrospray methods. The main drawback for its use as a microrobotic actuator is that a strong electric field is required to deform the liquid meniscus [on the order of kilovolts for a millimeter-size meniscus (42)]. Weaker electrical fields can be used to move a charged drop with negligible deformation of the interface by relying on electrophoresis (57).

3. MODELING AND CONTROL OF THE MENISCUS

The previous section focused on the passive point of view of the capillary effects; here, we address the questions of capillary system control both in open loop (involving a transducing table or map that links possible control parameters to their effect on the capillary system) and in closed loop (including sensors to monitor the capillary system status). The descriptions of the models and simulations enable a better understanding of the parameters.

3.1. Introductory Example

Let us illustrate the modeling problem on the typical axially symmetric sketch shown in **Figure 4**. A t-thick component is squeezed between a bottom passive meniscus (volume V_b) and a top active meniscus (volume V_t). The top meniscus is claimed to be active by controlling the contact angle θ_{tt} on the $z = h$ top surface (which could be done through different stimuli presented in **Figure 2**, such as electrowetting, UV light, or oxidoreduction of a surfactant). The modeling question is to find the geometrical shapes $r_b(z)$ and $r_t(z)$ of both menisci, and consequently the forces that they apply on the central component, or to find the conditions to fulfill the component equilibrium. At equilibrium, the geometry is defined by the Laplace law (Equation 2) linking the pressure gap across the meniscus interface and the meniscus curvature $2H$. In axially symmetric problems, the radius r of the meniscus depends only on z and the curvature:

$$\underbrace{2H = -\frac{r''}{(1+r'^2)^{\frac{3}{2}}} + \frac{1}{r(1+r'^2)^{\frac{1}{2}}}}_{\text{Curvature in axial symmetry}} \overbrace{=}^{\text{Laplace law}} \frac{p - \rho g z}{\gamma}, \qquad 4.$$

where $'$ and $''$ denote the first and second derivatives with respect to z, respectively; p is the pressure in the meniscus at the coordinate $z = 0$; ρ and γ are the liquid density and surface tension, respectively; and g is 9.81 m s^{-2}. For capillary problems in microrobotics, we will assume meniscus heights smaller than the capillary length L_C, which allows us to neglect the term $\rho g z$ and consider p to be constant in the meniscus. For dynamical problems, the picture is more complex, and the

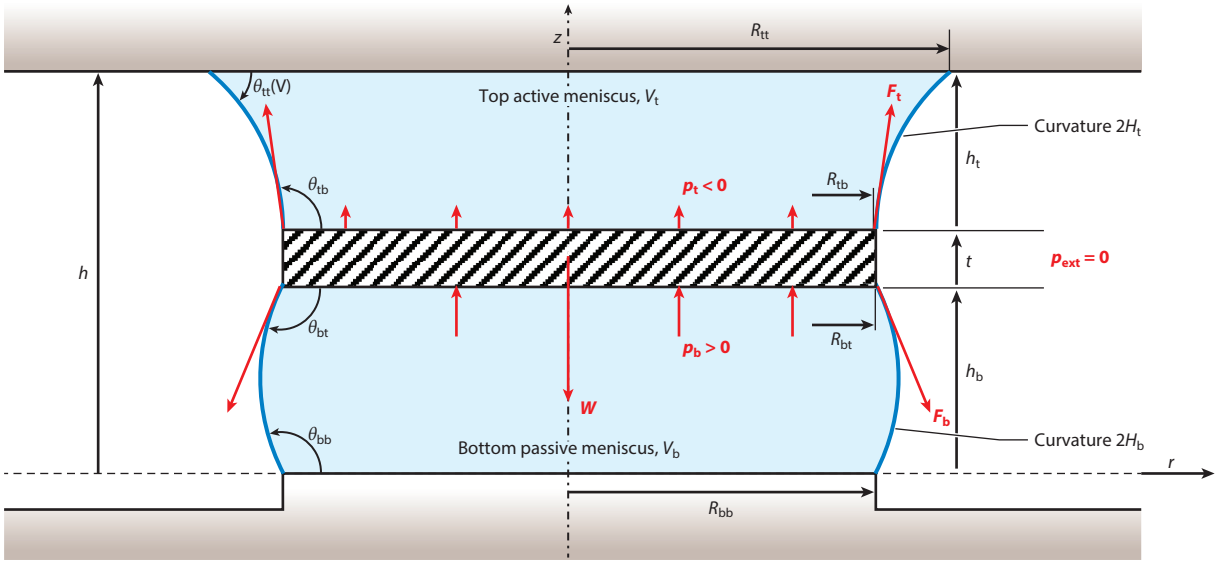

Figure 4

A companion model. The boundary conditions are the gap between the bottom and top surfaces, $h = h_b + t + h_t$; the contact angle, θ_b, or the pinning radius, $r_b(0) = R_{bb}$; the pinning radius on the bottom side of the component, $r_b(h_b) = R_{bt}$; the pinning radius on the top side of the component, $r_t(h_b + t) = R_{tb}$; the controlled contact angle, $\theta_{tt}(V)$, on the top surface, $z = h$; the fixed volume of liquid in the bottom passive meniscus, V_b; and the fixed volume of liquid in the top active meniscus, V_t. The b and t and subscripts refer to the top and bottom meniscus, respectively; the bb and bt subscripts refer to the bottom meniscus's bottom and top, respectively; and the tb and tt subscripts refer to the top meniscus's bottom and top, respectively.

full fluid mechanics problem must be solved, accounting for the presence of a free surface with surface tension (58) and sometimes with surface stresses induced by surfactants or temperature gradients (59). We further discuss the limits of a static simulation in Section 3.3.

In the (static) problem of **Figure 4**, we will therefore need to solve Equation 4 for both menisci, for which we use the boundary condition presented in the **Figure 4** caption. The vertical position h_b of the component is typically unknown, but the vertical equilibrium of the component can be expressed by the equilibrium of capillary forces (Laplace pressure component and surface tension component) and weight W:

$$\underbrace{\left(\overbrace{\pi R_{bt}^2 p_b}^{\text{Laplace pressure}} - \overbrace{2\pi R_{bt}\gamma \sin\theta_{bt}}^{\text{Surface tension}}\right)}_{\text{Force exerted by bottom meniscus}} + \underbrace{\left(-\pi R_{tb}^2 p_t + 2\pi R_{tb}\gamma \sin\theta_{tb}\right)}_{\text{Force exerted by top meniscus}} - W = 0, \qquad 5.$$

where the pressures p_b and p_t (assumed to be constant provided $h < L_C$) are related to the bottom and top meniscus curvatures $2H_b$ and $2H_t$, respectively. Equations 4 and 5 are second-order ordinary differential equations, requiring two initial conditions for each equation. Since the meniscus pressures p_b and p_t are not known in advance, this means that we need three conditions for each ordinary differential equation. The initial conditions can be read immediately from the physics [e.g., $r_b(0) = R_{bb}$] or adapted as boundary conditions provided that the meniscus heights h_b and h_t are known [e.g., $r_b(h_b) = R_{bt}$]. A book edited by Lambert (11) explained how to solve the problem with two embedded shooting methods in the case of one meniscus, provided that there exist a given gap and three boundary conditions (typically two contact angles and a volume of liquid).

In our example, the gap h_b must be guessed first (h_t is then derived from $h_t = h - h_b - t$) and iteratively adjusted to match the equilibrium represented by Equation 5.

3.2. Simulation Tools

Axially symmetric problems such as those shown in our companion example of **Figure 4** can be solved numerically using an ordinary differential equation solver (such as one provided in MATLAB or Python), as mentioned. Actually, this approach solves the static geometry of the meniscus, providing geometrical and pressure ingredients, from which the static capillary force can be calculated. This approach can sometimes be simplified by assuming a circular or parabolic meniscus shape. Strictly speaking, this simplification is not correct; however, it is reasonable in some cases, such as the circular approximation for meniscus aspect ratios, $h < r$ (which means that the second curvature term in Equation 4 can be neglected, along with the first one). A parabolic model is extremely useful when an analytical estimate is necessary for computing time issues. When the axial symmetry no longer holds (i.e., the full 3D problem), the problem must be solved by minimizing the surface energy under a constant volume constraint. The Surface Evolver software (60), which evolves an initial geometry toward energy minimization, is widely used for this purpose. For nonstatic problems (i.e., when viscous or inertial effects must be taken into account), a full fluid dynamics picture must be described and solved with relevant solvers (see, e.g., Reference 58 for the use of COMSOL software). A free surface is routinely included in solvers, while the tension component of capillary forces must still be added manually. Full 3D dynamical problems are still very hard to solve because of the computational time required.

Alternatively, a particle-based, mesh-free method can propose simulations with an intrinsic definition of the surface tension while by nature capturing the free surface. In a molecular dynamic simulation, each liquid molecule is simulated, and the surface tension arises from the intermolecular interaction forces (61). This simulation is particularly well suited for problems at the nanometer scale. From micro- to millimeter scales, particle-based simulation allows a fluid representation using a distribution of artificial liquid particles. The most popular is smoothed-particle hydrodynamics, where an interparticle force can be used to give an intrinsic definition of surface tension (62), thus removing the need for surface localization to apply the surface tension. This formulation has even been proposed to empirically model the dynamic contact angle (63). The advantages of particle-based methods are that they enable a conservative implementation (64) of the surface tension force, an easy fluid structure implementation (65), and a simple definition of the problem, as only the surface energies of the solid and the liquid need to be defined. The main disadvantages are the lack of an easy-to-use commercial solver and potentially slower calculation, as the equivalent of mesh refinement on a specific region of interest is currently impossible.

3.3. Static Versus Dynamic Problems

Static capillary problems are dominated mainly by surface tension, while dynamical features increase with increasing speeds or accelerations. Viscous or inertial effects can be compared with surface tension effects thanks to two well-known nondimensional numbers: the capillary number, $Ca = \frac{\mu v}{\gamma}$, which compares viscous and surface tension effects, and the Weber number, $We = \frac{\rho v^2 L}{\gamma}$, which compares inertia and surface tension effects, where μ is the fluid viscosity; L and v are the characteristic system size and speed, respectively; ρ is the fluid density; and γ is the surface tension. It is thus possible to position each system in a nondimensional *We–Ca* map such as those shown in **Figures 5** and **6**.

To fully exploit this map, we introduce a third nondimensional parameter that enables one to predict the evolution of a system when the velocity changes. Indeed, the displacement on the map due to an increase of the speed (or frequency) for a given system can be predicted by introducing

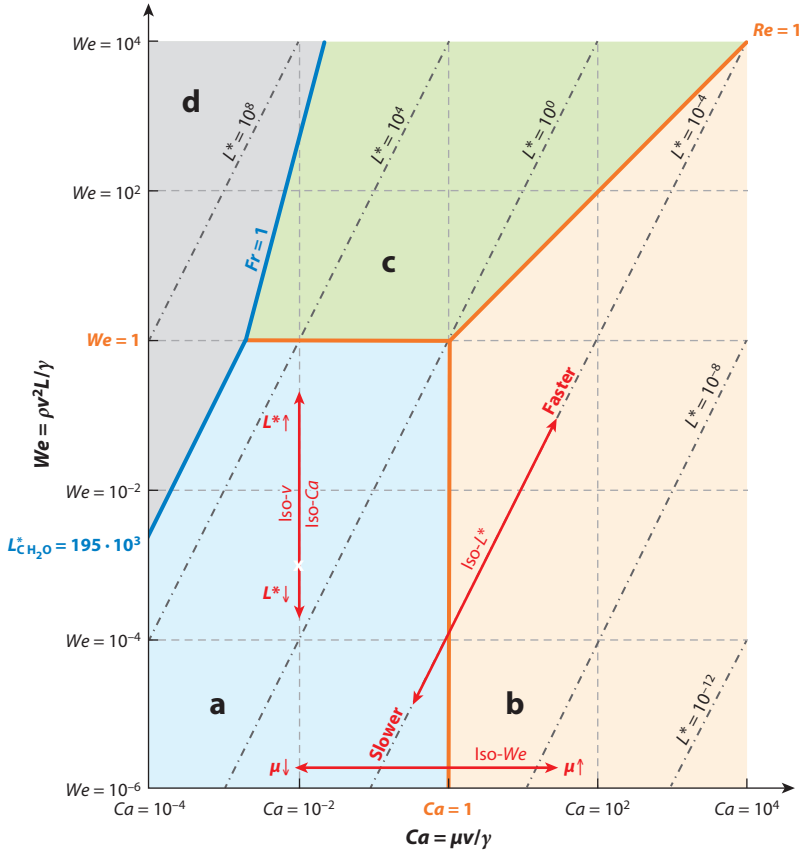

Figure 5

Nondimensional *We*–*Ca* map and isolines. Domain *a* (*light blue*) is dominated by surface tension, domain *b* (*light orange*) is dominated by viscosity, domain *c* (*light green*) is dominated by inertia, and domain *d* (*gray*) is dominated by gravity. The blue line indicates a nondimensional size $L^*_{\mathrm{C\,H_2O}} = 195 \cdot 10^3$ corresponding to the capillary length (the length below which the gravity effect is negligible compared with surface tension) for water and the limit $Fr = 1$. Changing the viscosity displaces working points horizontally along the iso-*We* line on the map (*We* does not depend on viscosity), changing the nondimensional size displaces points vertically along the iso-*Ca* line (changing L^* keeps velocity constant), and speeding the system up or down moves the working points along the iso-L^* slope-2 lines.

a nondimensional characteristic length L^*, defined by

$$L^* = \frac{L\rho\gamma}{\mu^2} = \frac{We}{Ca^2}, \qquad 6.$$

whose isocurves can be easily drawn in log scale as

$$\log We = 2\log Ca + \log L^*. \qquad 7.$$

As shown in **Figure 5**, it is thus possible to draw three series of isocurves (iso-L^*, iso-*Ca*, and iso-*We*), enabling one to predict the evolution of a system when the velocity v, dimension L, or viscosity μ is modified:

- Speed change: lines of slope 2, varying speed while keeping L^* constant (iso-L^*). The velocity increases when going up and to the right on the graph.

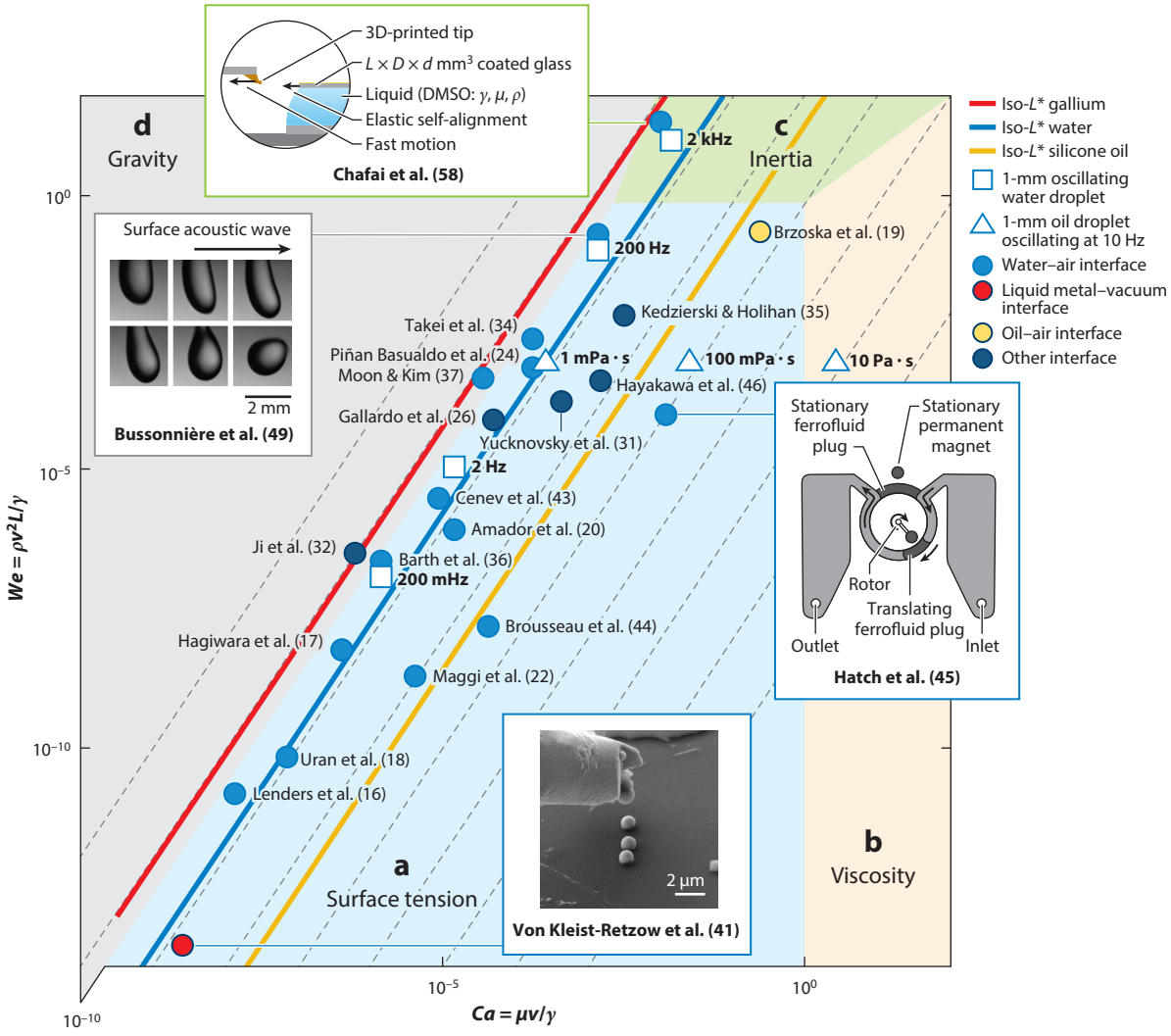

Figure 6

Nondimensional *We*–*Ca* map, with plain circles positioning works from literature. Most applications are in the capillary domain (domain *a*, *light blue*), and a few are in the inertial domain (domain *c*, *light green*). No works are listed in the viscous domain (domain *b*, *light orange*), which can be explained by the widespread use of water (high surface tension and low viscosity), rather than viscous oils (low surface tension and high viscosity). White squares indicate the positions of 1-mm-diameter oscillating droplets of 1-mPa·s-viscosity water at the frequency indicated in the figure. Note that an increase in frequency moves the different results along an iso-L^* line. Blue points indicate water–air interfaces, red points indicate liquid metal–vacuum interfaces, yellow points indicate oil–air interfaces, and dark blue points indicate other interfaces. White triangles correspond to 1-mm-diameter oil droplets (960 kg m^{-3}, 20 mN m^{-1}) at 10 Hz, with a viscosity indicated in the figure. The red, blue, and yellow lines correspond to iso-L^* for gallium ($L^* = 7.76 \cdot 10^6$), water ($L^* = 195 \cdot 10^3$), and silicone oil ($L^* = 280$), respectively. Abbreviation: DMSO, dimethyl sulfoxide. Insets adapted with permission from References 41, 45, 49, and 58, respectively.

- Length change: vertical lines, varying L while keeping Ca constant (iso-Ca). Reducing the size of a system means going down on the graph.
- Viscosity change: horizontal lines, varying viscosity μ while keeping We constant (iso-We). The viscosity increases when going to the right on the graph.

This map also enables one to identify several domains, taking into account some physical frontiers. The two first frontiers are defined by the nondimensional numbers $Ca = 1$ and $We = 1$. One of the frontiers is also linked to the Reynolds number, $Re = We/Ca = \frac{\rho v L}{\mu} = 1$. The fourth frontier is linked to the capillary length L_C (Equation 1). Indeed, it is possible to calculate the nondimensional capillary length L_C^* by combining Equations 1 and 7:

$$L_C^* = \frac{L_C \rho \gamma}{\mu^2} = \frac{We}{Ca^2}, \quad 8.$$

where for water, the numerical value is $L_C^* = 195 \cdot 10^3$, as shown in **Figure 5**. A last limit is represented by the Froude number, $Fr = \frac{v}{\sqrt{gl}}$, introducing the balance between the inertia and gravitational force. It is possible to show that

$$\frac{Ca^4}{We} = g^* \cdot Fr^2, \quad 9.$$

where $g^* = \frac{g\mu^4}{\rho\gamma^3}$ (in the case of water, $g^* = 26 \cdot 10^{-12}$). The limit $Fr = 1$ is thus a line with a slope of 4 on the nondimensional map (see **Figure 5**), defined by

$$\log We = 4 \log Ca + \log g^*. \quad 10.$$

We can therefore identify four domains in a nondimensional map such as the one shown in **Figure 5**: the static capillary domain, when $Ca < 1$, $We < 1$, and $L^* < L_C^*$, where surface tension dominates the other effects (domain *a*); the viscous domain, when $Ca > 1$ and $Re < 1$ (domain *b*); the inertial domain, when $We > 1$, $Re > 1$, and $Fr > 1$ (domain *c*); and the gravity-driven domain, when either $We < 1$ and $L^* > L_C^*$ or $We > 1$ and $Fr < 1$ (domain *d*).

Each new problem or each reference from the literature can therefore be assessed in terms of Ca and We once their underlying parameters are identified: μ, v, L, ρ, and γ (see **Figure 6**). For instance, we see on the map that the Dropbot platform developed by Lenders et al. (16) is slow and small enough to be modeled statically, while the capillary self-alignment reported by Chafai et al. (58) is too fast to be modeled statically. This analysis considers the order of magnitude of both the size and the velocity and does not highlight the transition between asymptotic regimes (e.g., $We \gg 1$ and $We \ll 1$). Indeed, the limit of the inertial regime appears around $We = 1$ but not exactly at $We = 1$ (and, similarly, the viscous regime transition appears at $Ca = 1$). As an example, Bussonnière et al. (49) reported some dynamical effects at $We = 0.28$.

3.4. Sensing

For both characterization and control, the essential information about the state of an actuator is its force and displacement. As presented in the companion model in **Figure 4** and in Equation 5, both values are linked. Indeed, from the overall liquid meniscus shape (and hence its displacement), the force can be deduced by summing the contribution of the liquid inner pressure and triple-line tension (Equation 5).

For the characterizations of the system for either design optimization or model construction, the simple approach is often to use off-the-shelf characterization tools. For the displacement, microscope image analyses are enough, with a maximal resolution above 1 μm. Measuring smaller displacements or reaching higher frequencies requires either optical sensors or direct contact. The force can be measured directly with sensors, and in microrobotics, most force sensors are based on an elastic deformation measured by different techniques: deflection of a laser beam, in the case of an atomic force microscope and surface force apparatus (66); strain gauges; noncontact displacement sensors; or capacitive measurement. Alternatively, a good measurement of the meniscus geometry can serve to compute the force on the effector. Indeed, the pressure

can be deduced from the meniscus radius of curvature at one point [by using the Laplace law (Equation 4)], and then the force can be deduced by measuring the wet area and the contact angle of the triple line on either the actuator or the effector (by using Equation 5).

These kinds of measurements allow the validation or construction of a model to facilitate the development of open-loop systems. However, the large footprints of the sensors and the need to align them with the liquid meniscus mechanism prohibit their use during practical applications. Therefore, proprioceptive sensors (i.e., sensors embedded in the actuator) are required to develop closed-loop actuators for microrobotic applications. One of the great advantages of liquid meniscus actuators is that the presence of liquid allows a wide variety of robust proprioceptive sensing approaches:

- Pressure: The liquid ensures that the inner pressure is the same in all of the liquid (when working under the capillary length), therefore requiring only one measure at the most convenient point (a channel can be designed for this specific application) (15). Pressure measurement is potentially easy to miniaturize (67). Measuring the deformation of a membrane or simply of another interface and deducing the pressure value from Laplace's law is also possible.
- Light: Because the smooth shape of a liquid interface gives it exceptionally good optical properties, it can be used as, e.g., a lens (68) or optical cavity (69). This approach allows a measurement of the curvature of the interface, which can be linked to the pressure. Liquid lenses such as the one developed by Varioptic are a particularly good example of closed-loop control of a liquid meniscus shape. Indeed, by treating this system as an actuator, the autofocus algorithm of the lens guarantees closed-loop control of the meniscus position. From a technological point of view, light has good proprioceptive potential, as it can easily be guided in optical fiber.
- Electricity: Liquid can potentially conform to any shape while guaranteeing an electrical connection. Large-displacement sensors also use liquid as a resistive element. The simple resistivity of the liquid meniscus has been proposed as a way to measure its deformation (70), and an impedance sensor based on a fluid meniscus has also been proposed (71). By placing many electrodes on a single meniscus, methods inspired by electrical impedance tomography (72) could be used to reconstruct the complex drop geometry and hence the full 3D force and torque applied on the effector.

3.5. Control of Capillary Microrobots

The description of the control strategy is linked to the general architecture of the capillary-based actuator. Two major cases can be considered: (*a*) The manipulated object or the moving part of the actuator has a size comparable to that of the droplet, and (*b*) the manipulated object is placed on a liquid interface whose surface is significantly larger than the object surface. In the first case, the droplet acts as an actuator, and in the second case, the moving object can be considered a mobile microrobot walking on the liquid interface.

3.5.1. Robots based on fluid joints. When using a capillary bridge as an actuator, different approaches to controlling the shape of the droplet have been explored in the literature. The general objective is to be able to guarantee performance (position, curvature, etc.) despite the nonlinearities of the microdroplets' behavior. Indeed, the link between the actuation physical variable [e.g., voltage in the case of an electrowetting-on-dielectric (EWOD)–actuated microdroplet] and the objective displacement or force (e.g., the curvature of the droplet in an active

lens) is highly nonlinear. Moreover, the surface-angle hysteresis and the possible evaporation of the droplets induce, respectively, a hysteresis and a drift in the microdroplet-based actuators.

The first approach consists of (*a*) focusing on the design of the system in order to reduce as much as possible the impact of the nonlinearities on the system behavior and (*b*) designing actuators with many natural equilibria, thus allowing discrete commands between those positions. The basic principle is the self-assembly of micro-objects placed on a matrix of microdroplets. The design of the droplets enables one to position the object above the droplet automatically, without external control (73–75). EWOD enables one to move the droplet along several stable positions and thus move the object above the droplet. In such a case, the system is discrete, and the control is usually an open-loop discrete control (without sensor feedback). This technique enables both linear (34, 35) and rotational (35, 37) actuators.

The second approach is to consider the droplet to be a continuous actuator, enabling one to reach an infinite number of positions. One of the examples is to use the droplet as a microlens whose curvature can be controlled. These systems are usually controlled in open loop using a feedforward controller based on the physical model of the actuator (44, 68). When the microdroplet is used to actuate a tool (e.g., a microgripper), the system is controlled using a teleoperation approach in which the user can visualize the actuator position using visual feedback and can adjust the position of the actuator (15, 16, 25, 36). This teleoperation mode opens the way to full automatic control using closed-loop control (15, 16), enabling one to guarantee performance without human intervention. The major challenge is the development of real-time perception aims, where two major options have been foreseen: photosensing (70) and resistive/capacitive sensing (70, 76).

3.5.2. Mobile microrobots at the fluid–fluid interface. The fluid–fluid interface—and, more specifically, the air–water interface—has drawn huge interest in recent years for the manipulation of mobile microrobots, as it avoids dry friction (which is present in ambient environments), leading to increased repeatability, and reduces viscous drag compared with manipulation in liquid, leading to huge velocities. Thanks to surface tension, microrobots denser than water float on the surface and can be actuated by various means.

One option relies on the deformation of the interface using ferrofluids. Magnetic fields are tuned to create bumps on the surface of the liquid. The motion of the microrobot can be predicted by considering the total energy of the system, composed of gravitational, capillary, and magnetic contributions. To minimize this energy, the microrobot moves away from these bumps, the height of which can be on the order of hundreds of micrometers (43). The generation of a gradient of surface tension is a second option to induce a flow displacement used to control the position of the microrobot. Surface tension is locally decreased by using solvents or surfactants (77) or by locally heating the surface with a laser (24). The microrobot is repelled from areas with low surface tension.

In all of these cases, the microrobots are repelled, leading to an unstable system that must be controlled in closed loop. Model-based control, mostly obtained experimentally, is commonly used with vision-based feedback. However, the motion is highly dependent on the environmental conditions (the composition of the liquid, concentration of the surfactants, temperature of the liquid, air flows, etc.), which are considered perturbations in the control. Alternatively, a magnetic gradient can generate a 2D stable equilibrium, allowing the trapping of ferromagnetic or magnetic mobile microrobots; in this case, the control is straightforward, as the robot's in-plane displacement corresponds to the magnet's displacement (78).

In addition to these perturbations, some issues are specific to the actuation means. The deformation of the interface makes it difficult to independently control several microrobots. Regarding the use of a gradient of surface tension, the actuation itself modifies the environment

(the concentration of surfactants or the temperature) and thus the boundary conditions of the model. Trajectories that go to the same place several times in a short period are challenging and should be avoided by planning, or one takes the risk of losing the precision and even the efficiency (the surface tension gradient might tend to zero) of the control.

4. APPLICATIONS OF THE MENISCUS TO MICROROBOTICS

Surface tension–based applications cover not only technologically complex developments (based on microfabrication, advanced texturation, and coatings) but also elegant and straightforward solutions, where a simple fluid meniscus can compete with and even exceed the performance of well-designed grippers, mechanical joints, and actuators that require specific different parts. Moreover, as illustrated in **Figure 7**, the fluid interface is able to realize several functions in a system

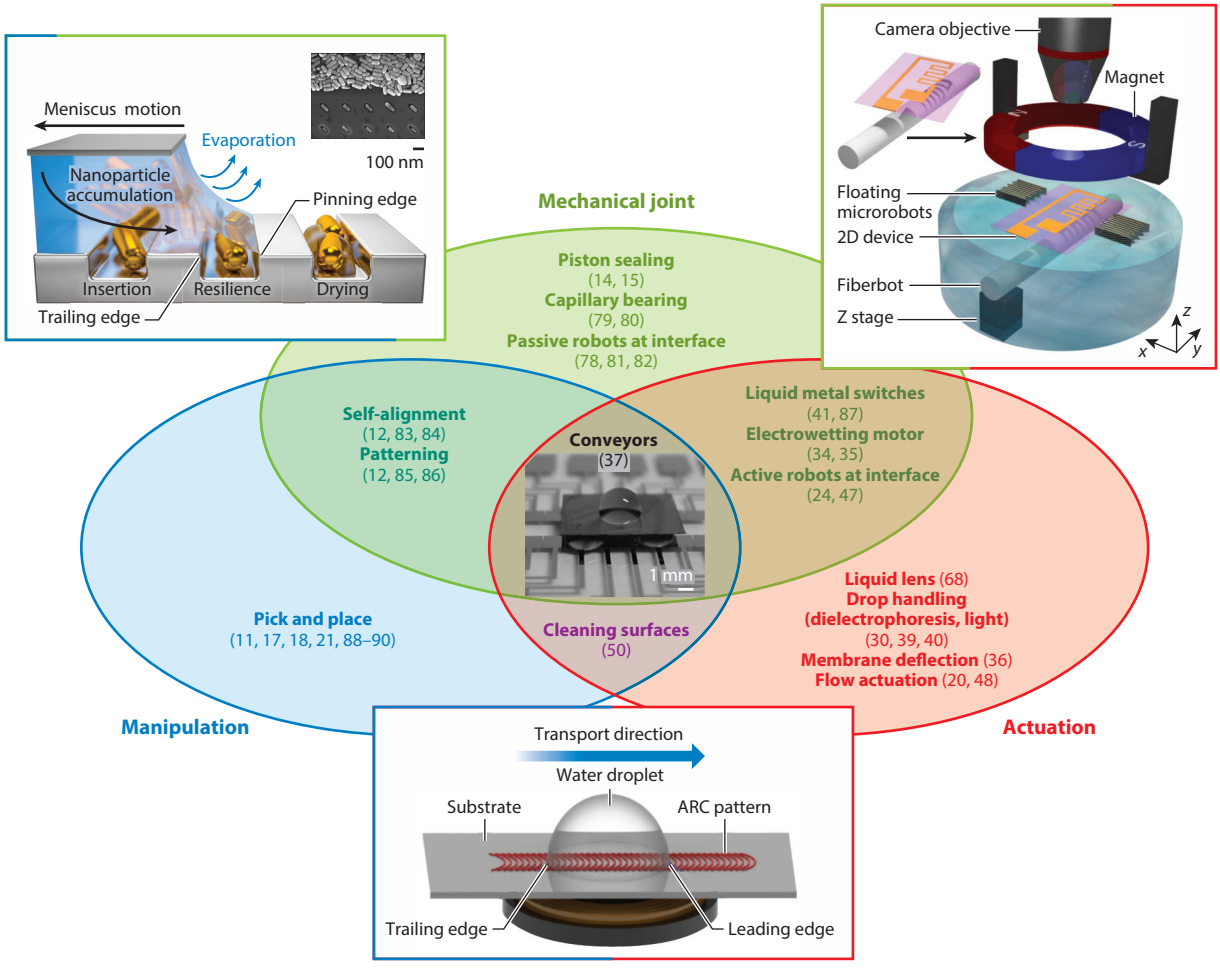

Figure 7

Classification of different liquid meniscus applications using three categories: mechanical joints (*green*), manipulation (*blue*), and actuation (*red*). Abbreviation: ARC, anisotropic ratchet conveyor. Top left inset adapted with permission from Reference 89; top right inset adapted with permission from Reference 78; bottom inset adapted from Reference 50 (CC BY 4.0); center inset adapted with permission from Reference 37.

and therefore reduces the design complexity in a comparable way as soft robots. This is a great advantage, as fabrication and assembly constraints increase with size reduction, rendering complex assembly of different parts impossible.

As presented in **Figure 7**, surface tension in microrobotics can first be used as mechanical joints. It has been proposed, for example, as a 1D mechanical joint without a restoring force to ensure linear translation and sealing in a micropiston for use in minimally invasive surgery (14, 15). Still in 1D, the rotation of a magnetic motor maintained by a liquid meniscus has been demonstrated (79). Floating robots at the fluid interface use the meniscus as a 3D mechanical joint (two translational dimensions and one rotational dimension) (78, 80, 81). The restoring force of the liquid meniscus can also be used and tuned to provide a well-modeled force that enables large displacements compared with the usual solid deformation used at this scale (82).

As actuators, fluid menisci have been successfully used in a liquid lens (68). Indeed, the smooth molecular surface provides excellent natural optical properties at a low fabrication cost, and the actuation of the interface allows fast focus without mechanical moving parts. The use of moving droplets is also an important application field, particularly for microfluidic chips, where each droplet acts as an independent chemical reactor (30, 39, 40). However, although many ways of moving droplets have been proposed, merging and splitting of droplets remain challenging. Fluid menisci can also be used to actuate a membrane deflection by using the associated change of pressure inside the liquid meniscus (thus increasing the deflection, as the membrane stiffness can be lower than the liquid surface tension) (36). Finally, a liquid interface can be used to generate a flow inside a microfluidic chip (20) or a propelling flow to control a miniaturized catheter in a fluid medium (48).

The use of surface tension has also been proposed in microrobotics to manipulate objects. Indeed, for the same reason that one can lick a finger to get a better grasp on a paper sheet, a liquid meniscus makes a naturally compliant gripper. This use has been demonstrated for pick and place of small components (83, 84), including those with complex shapes (17). As a method of releasing an object, evaporation of liquid has been suggested (18, 21). A similar approach can be used in a liquid medium with an air bubble embedded in a magnetic microrobot and acting as a gripper (85).

As previously mentioned, one advantage of liquid menisci is that they can serve multiple purposes in a single design. Indeed, in applications as both a mechanical joint and actuator, liquid menisci were shown to propel a robot constrained to the water interface through thermocapillary actuation (24) or the addition of a surfactant (47). Electrowetting linear (35) and rotating (34) motors also use the meniscus as both a mechanical joint and actuator and provide a significant force relative to their footprint. Finally, a meniscus can be utilized as a controllable electrical switch by using liquid metal as the meniscus liquid (41, 86). Combining meniscus actuation with manipulation has also been proposed for vibration-induced cleaning of surfaces, using a single drop that can move across a solar panel surface and collect dust (50).

The self-alignment of parts linked by a liquid meniscus combines the mechanical joint and manipulation properties. This method has been proposed for the assembly and alignment of individual microcomponents in electronics (87, 88) and could potentially be extended to a larger scale, as the alignment is purely passive (12), allowing it to achieve parallel nanoscale manipulation and assembly for patterning purposes. It has been demonstrated using only the capillary force on a gold nanorod (89) as well as in combination with dielectrophoresis for patterning on a single carbon nanotube (90).

Finally, a microconveyor system where a substrate is supported by four drops that can move on a substrate thanks to an electrowetting system has demonstrated the ability to use the fluid meniscus as a mechanical joint and actuator for the manipulation of a microplatform (37).

5. CHALLENGES, CONCLUSIONS, AND PERSPECTIVES

Building on a brief historical description of capillary phenomena, this article has provided a three-part perspective on the inclusion of surface tension effects in microsystems: physical models, control and sensing schemes, and applications. The tools and information presented here will be useful to researchers seeking to build elegant and simple systems below the capillary length, as a single liquid meniscus can serve many purposes.

The liquid meniscus is also an interesting candidate for the development of complex actuators below the micrometer scale. While the capillary length has been identified as the upper boundary of a soft/wet microrobotics regime, a lower boundary could be defined with the so-called Kelvin radius (9), which for water at 20°C is approximately 5 nm. Of course, at such a small scale, sensing the meniscus to provide the information necessary for closed-loop control might be extremely challenging, but manipulation in a scanning electron microscope with imaging feedback has already been reported (41). Whatever the exact limit, extreme care will be given to mastering the boundary conditions, especially the sharpness of the edges that confine droplets and menisci as well as controlled and sustainable wetting properties.

All of this opens up new possibilities for soft/wet microrobotics, even going beyond conventional water menisci to make use of more exotic liquids, such as liquid metals and salt, glue, and ferrofluids. Fluids with non-Newtonian properties could also be used to present naturally complex mechanical responses to an external control parameter.

DISCLOSURE STATEMENT

The authors are not aware of any affiliations, memberships, funding, or financial holdings that might be perceived as affecting the objectivity of this review.

LITERATURE CITED

1. Jurin J. 1718. An account of some experiments shown before the Royal Society: with an enquiry into the cause of ascent and suspension of water in capillary tubes. *Philos. Trans. R. Soc.* 30:739–47
2. Feng S, Zhu P, Zheng H, Zhan H, Chen C, et al. 2021. Three-dimensional capillary ratchet-induced liquid directional steering. *Science* 373:1344–48
3. Laplace PS. 1805. *Supplément au dixième livre du Traité de mécanique céleste. Sur l'action capillaire*. Paris: Courcier
4. Plateau JAF. 1873. *Statique expérimentale et théorique des liquides soumis aux seules forces moléculaires*. Paris: Gauthier-Villars
5. Wenzel RN. 1936. Resistance of solid surfaces to wetting by water. *Ind. Eng. Chem.* 28:988–94
6. Washburn E. 1921. The dynamics of capillary flow. *Phys. Rev.* 17:273–83
7. Tanner LH. 1979. The spreading of silicone oil drops on horizontal surfaces. *J. Phys. D* 12:1473–84
8. Adamson AW, Gast AP. 1997. *Physical Chemistry of Surfaces*. New York: Wiley & Sons. 6th ed.
9. Israelachvili JN. 1992. *Intermolecular and Surface Forces*. San Diego, CA: Academic. 2nd ed.
10. de Gennes PG, Brochart-Wyard F, Quéré D. 2002. *Gouttes, bulles, perles et ondes*. Paris: Belin
11. Lambert P, ed. 2013. *Surface Tension in Microsystems: Engineering Below the Capillary Length*. Berlin: Springer
12. Mastrangeli M, Zhou Q, Sariola V, Lambert P. 2017. Surface tension-driven self-alignment. *Soft Matter* 13:304–27
13. Brakke K. 1992. The surface evolver. *Exp. Math.* 1:141–65
14. De Volder M, Peirs J, Reynaerts D, Coosemans J, Puers R, et al. 2005. A novel hydraulic microactuator sealed by surface tension. *Sens. Actuators A* 123–24:547–54
15. Barbot A, Power M, Seichepine F, Yang GZ. 2020. Liquid seal for compact micropiston actuation at the capillary tip. *Sci. Adv.* 6:eaba5660

16. Lenders C, Gauthier M, Cojan R, Lambert P. 2012. Three-DOF microrobotic platform based on capillary actuation. *IEEE Trans. Robot.* 28:1157–61
17. Hagiwara W, Ito T, Tanaka K, Tokui R, Fuchiwaki O. 2019. Capillary force gripper for complex-shaped micro-objects with fast droplet forming by on–off control of a piston slider. *IEEE Robot. Autom. Lett.* 4:3695–702
18. Uran S, Šafaric R, Bratina B. 2017. Reliable and accurate release of micro-sized objects with a gripper that uses the capillary-force method. *Micromachines* 8:182
19. Brzoska J, Brochard-Wyart F, Rondelez F. 1993. Motions of droplets on hydrophobic model surfaces induced by thermal gradients. *Langmuir* 9:2220–24
20. Amador GJ, Tabak AF, Ren Z, Alapan Y, Yasa O, Sitti M. 2018. Thermocapillary-driven fluid flow within microchannels. arXiv:1802.00475 [physics.flu-dyn]
21. Iazzolino A, Tourtit Y, Chafai A, Gilet T, Lambert P, Tadrist L. 2019. Pick up and release of micro-objects: a motion-free method to change the conformity of a capillary contact. *Soft Matter* 16:754
22. Maggi C, Saglimbeni F, Dipalo M, De Angelis F, Di Leonardo R. 2015. Micromotors with asymmetric shape that efficiently convert light into work by thermocapillary effects. *Nat. Commun.* 6:6–10
23. Zhang J, Wang Z, Wang Z, Zhang T, Wei L. 2019. In-fibre particle manipulation and device assembly via laser induced thermocapillary convection. *Nat. Commun.* 10:5206
24. Piñan Basualdo FN, Bolopion A, Gauthier M, Lambert P. 2021. A microrobotic platform actuated by thermocapillary flows for manipulation at the air-water interface. *Sci. Robot.* 6:eabd3557
25. Hu W, Ishii KS, Ohta AT. 2011. Micro-assembly using optically controlled bubble microrobots. *Appl. Phys. Lett.* 99:094103
26. Gallardo BS, Gupta VK, Eagerton FD, Jong LI, Craig VS, et al. 1999. Electrochemical principles for active control of liquids on submillimeter scales. *Science* 283:57–60
27. Wissman J, Dickey MD, Majidi C. 2017. Field-controlled electrical switch with liquid metal. *Adv. Sci.* 4:1700169
28. Läubli NF, Burri JT, Marquard J, Vogler H, Mosca G, et al. 2021. 3D mechanical characterization of single cells and small organisms using acoustic manipulation and force microscopy. *Nat. Commun.* 12:2583
29. Shin JY, Abbott NL. 1999. Using light to control dynamic surface tensions of aqueous solutions of water soluble surfactants. *Langmuir* 15:4404–10
30. Diguet A, Guillermic RM, Magome N, Saint-Jalmes A, Chen Y, et al. 2009. Photomanipulation of a droplet by the chromocapillary effect. *Angew. Chem.* 48:9281–84
31. Yucknovsky A, Rich BB, Westfried A, Pokroy B, Amdursky N. 2021. Self-propulsion of droplets via light-stimuli rapid control of their surface tension. *Adv. Mater. Interfaces* 8:2100751
32. Ji W, Li W, Wang Y, Lan D. 2019. Tunable spreading and shrinking on photocontrolled liquid substrate. *ACS Omega* 4:21967–74
33. Rosario R, Gust D, Hayes M, Jahnke F, Springer J, Garcia AA. 2002. Photon-modulated wettability changes on spiropyran-coated surfaces. *Langmuir* 18:8062–69
34. Takei A, Matsumoto K, Shomoyama I. 2010. Capillary motor driven by electrowetting. *Lab Chip* 10:1781
35. Kedzierski J, Holihan E. 2018. Linear and rotational microhydraulic actuators driven by electrowetting. *Sci. Robot.* 3:eaat5643
36. Barth CA, Hu X, Mibus MA, Reed ML, Knospe CR. 2018. Large membrane deflection via capillary force actuation. *J. Micromech. Microeng.* 28:065008
37. Moon I, Kim J. 2006. Using EWOD (electrowetting-on-dielectric) actuation in a micro conveyor system. *Sens. Actuators A* 130:537–44
38. Velev OD, Prevo BG, Bhatt KH. 2003. On-chip manipulation of free droplets. *Nature* 426:515–16
39. Chatterjee D, Shepherd H, Garrell RL. 2009. Electromechanical model for actuating liquids in a two-plate droplet microfluidic device. *Lab Chip* 9:1219–29
40. Daunay B, Lambert P, Jalabert L, Kumemura M, Renaudot R, et al. 2012. Effect of substrate wettability in liquid dielectrophoresis (LDEP) based droplet generation: theoretical analysis and experimental confirmation. *Lab Chip* 12:361–68
41. von Kleist-Retzow FT, Haenssler OC, Fatikow S. 2018. Manipulation of liquid metal inside an SEM by taking advantage of electromigration. *J. Microelectromech. Syst.* 28:88–94

42. Li J. 2006. On the meniscus deformation when the pulsed voltage is applied. *J. Electrostat.* 64:44–52
43. Cenev Z, Harischandra PD, Nurmi S, Latikka M, Hynninen V, et al. 2021. Ferrofluidic manipulator: automatic manipulation of nonmagnetic microparticles at the air–ferrofluid interface. *IEEE/ASME Trans. Mechatron.* 26:1932–40
44. Brousseau D, Borra EF, Jean-Ruel H, Parent J, Ritcey A. 2006. A magnetic liquid deformable mirror for high stroke and low order axially symmetrical aberrations. *Opt. Express* 14:11486
45. Hatch A, Kamholz AE, Holman G, Yager P, Böhringer KF. 2001. A ferrofluidic magnetic micropump. *J. Microelectromech. Syst.* 10:215–21
46. Hayakawa M, Vialetto J, Anyfantakis M, Takinoue M, Rudiuk S, et al. 2019. Effect of moderate magnetic fields on the surface tension of aqueous liquids: a reliable assessment. *RSC Adv.* 9:10030
47. Jin H, Marmur A, Ikkala O, Ras RH. 2012. Vapour-driven marangoni propulsion: continuous, prolonged and tunable motion. *Chem. Sci.* 3:2526–29
48. Qiu T, Adams F, Palagi S, Melde K, Mark A, et al. 2017. Wireless acoustic-surface actuators for miniaturized endoscopes. *ACS Appl. Mater. Interfaces* 9:42536–43
49. Bussonnière A, Baudoin M, Brunet P, Matar OB. 2016. Dynamics of sessile and pendant drops excited by surface acoustic waves: gravity effects and correlation between oscillatory and translational motions. *Phys. Rev. E* 93:053106
50. Sun D, Böhringer KF. 2020. An active self-cleaning surface system for photovoltaic modules using anisotropic ratchet conveyors and mechanical vibration. *Microsyst. Nanoeng.* 6:87
51. Berry S, Kedzierski J, Abedian B. 2006. Low voltage electrowetting using thin fluoroploymer films. *J. Colloid Interface Sci.* 303:517–24
52. Xia Y, Song C, Meng Y, Xue P, DeMello AJ, et al. 2022. An addressable electrowetting valve for centrifugal microfluidics. *Sens. Actuators B* 369:132276
53. Hao C, Liu Y, Chen X, He Y, Li Q, et al. 2014. Electrowetting on liquid-infused film (EWOLF): complete reversibility and controlled droplet oscillation suppression for fast optical imaging. *Sci. Rep.* 4:6846
54. Chiou PY, Moon H, Toshiyoshi H, Kim CJ, Wu MC. 2003. Light actuation of liquid by optoelectrowetting. *Sens. Actuators A* 104:222–28
55. Pei SN, Valley JK, Neale SL, Jamshidi A, Hsu HY, Wu MC. 2010. Light-actuated digital microfluidics for large-scale, parallel manipulation of arbitrarily sized droplets. In *2010 IEEE 23rd International Conference on Micro Electro Mechanical Systems (MEMS)*, pp. 252–55. Piscataway, NJ: IEEE
56. Sato H, Kaji N, Mochizuki T, Mori YH. 2006. Behavior of oblately deformed droplets in an immiscible dielectric liquid under a steady and uniform electric field. *Phys. Fluids* 18:127101
57. Im DJ. 2015. Next generation digital microfluidic technology: electrophoresis of charged droplets. *Korean J. Chem. Eng.* 32:1001–8
58. Chafai A, Vitry Y, Dehaeck S, Gallaire F, Scheid B, et al. 2021. Two-dimensional modelling of transient capillary driven damped micro-oscillations and self-alignment of objects in microassembly. *J. Fluid Mech.* 910:A6
59. Piñan Basualdo F, Terrazas Mallea R, Scheid B, Bolopion A, Gauthier M, Lambert P. 2021. Effect of insoluble surfactants on a thermocapillary flow. *Phys. Fluids* 33:072106
60. Brakke KA. 1996. The surface evolver and the stability of liquid surfaces. *Philos. Trans. R. Soc. A* 354:2143–57
61. Becker S, Urbassek HM, Horsch M, Hasse H. 2014. Contact angle of sessile drops in Lennard-Jones systems. *Langmuir* 30:13606–14
62. Tartakovsky A, Meakin P. 2005. Modeling of surface tension and contact angles with smoothed particle hydrodynamics. *Phys. Rev. E* 72:026301
63. Bao Y, Li L, Shen L, Lei C, Gan Y. 2019. Modified smoothed particle hydrodynamics approach for modelling dynamic contact angle hysteresis. *Acta Mech. Sin.* 35:472–85
64. Kondo M, Matsumoto J. 2021. Surface tension and wettability calculation using density gradient potential in a physically consistent particle method. *Comput. Methods Appl. Mech. Eng.* 385:114072
65. Akinci N, Akinci G, Teschner M. 2013. Versatile surface tension and adhesion for SPH fluids. *ACM Trans. Graph.* 32:182
66. Israelachvili JN, Min Y, Akbulut M, Alig A, Carver G, et al. 2010. Recent advances in the surface forces apparatus (SFA) technique. *Rep. Prog. Phys.* 73:036601

67. Song P, Ma Z, Ma J, Yang L, Wei J, et al. 2020. Recent progress of miniature MEMS pressure sensors. *Micromachines* 11:56
68. Gabay C, Berge B, Dovillaire G, Bucourt S. 2002. Dynamic study of a Varioptic variable focal lens. In *Current Developments in Lens Design and Optical Engineering III*, ed. RE Fischer, WJ Smith, RB Johnson, pp. 159–65. Bellingham, WA: SPIE
69. Giorgini A, Avino S, Malara P, De Natale P, Gagliardi G. 2019. Liquid droplet microresonators. *Sensors* 19:473
70. Casier R, Lenders C, Lhernould MS, Gauthier M, Lambert P. 2013. Position measurement/tracking comparison of the instrumentation in a droplet-actuated-robotic platform. *Sensors* 13:5857–69
71. Nie B, Xing S, Brandt JD, Pan T. 2012. Droplet-based interfacial capacitive sensing. *Lab Chip* 12:1110–18
72. Avery J, Runciman M, Darzi A, Mylonas GP. 2019. Shape sensing of variable stiffness soft robots using electrical impedance tomography. In *2019 International Conference on Robotics and Automation (ICRA)*, pp. 9066–72. Piscataway, NJ: IEEE
73. Takei A, Matsumoto K, Shimoyama I. 2009. Capillary torque caused by a liquid droplet sandwiched between two plates. *Langmuir* 26:2497–504
74. Sariola V, Jääskeläinen M, Zhou Q. 2010. Hybrid microassembly combining robotics and water droplet self-alignment. *IEEE Trans. Robot.* 26:965–77
75. Mastrangeli M, Abbasi S, Varel C, Hoof CV, Celis JP, Böhringer KF. 2009. Self-assembly from milli- to nanoscales: methods and applications. *J. Micromech. Microeng.* 2009:083001
76. Hu X, Mibus M, Zangari G, Knospe C, Reed ML. 2015. Interrogation of droplet configuration during electrowetting via impedance spectroscopy. *IEEE J. Microelectromech. Syst.* 24:2092–100
77. Pena-Francesch A, Giltinan J, Sitti M. 2019. Multifunctional and biodegradable self-propelled protein motors. *Nat. Commun.* 10:3188
78. Barbot A, Tan H, Power M, Seichepine F, Yang GZ. 2019. Floating magnetic microrobots for fiber functionalization. *Sci. Robot.* 4:eaax8336
79. He Y, Wang L, Li Q, Yang L, Rong W, Sun L. 2019. Characterization of rotary magnetic micromotor supported on single droplet. *J. Micromech. Microeng.* 29:125010
80. He Y, Wang L, Zhao M, Fan Z, Rong W, Sun L. 2022. Flexible magnetic micropartners for micromanipulation at interfaces. *ACS Appl. Mater. Interfaces* 14:22570–81
81. Zhang X, Zhao J, Zhu Q, Chen N, Zhang M, Pan Q. 2011. Bioinspired aquatic microrobot capable of walking on water surface like a water strider. *ACS Appl. Mater. Interfaces* 3:2630–36
82. Ni Q, Crane N. 2018. Controlling normal stiffness in droplet-based linear bearings. *Micromachines* 9:525
83. Bark C, Binnenboese T. 1998. Gripping with low viscosity fluids. In *The Eleventh Annual International Workshop on Micro Electro Mechanical Systems*, pp. 301–5. Piscataway, NJ: IEEE
84. Pagano C, Zanoni L, Fassi I, Jovane F. 2006. Micro-assembly: design and analysis of a gripper based on capillary force. In *Proceedings of the First CIRP International Seminar on Assembly Systems*, pp. 165–70. Stuttgart, Ger.: Inst. Ind. Manuf. Manag., Univ. Stuttgart
85. Giltinan J, Diller E, Sitti M. 2016. Programmable assembly of heterogeneous microparts by an untethered mobile capillary microgripper. *Lab Chip* 16:4445–57
86. Ye Z, Lum GZ, Song S, Rich S, Sitti M. 2016. Phase change of gallium enables highly reversible and switchable adhesion. *Adv. Mater.* 28:5088–92
87. Chang B, Sariola V, Jääskeläinen M, Zhou Q. 2010. Self-alignment in the stacking of microchips with mist-induced water droplets. *J. Micromech. Microeng.* 21:015016
88. Xiong X, Hanein Y, Fang J, Wang Y, Wang W, et al. 2003. Controlled multibatch self-assembly of microdevices. *J. Microelectromech. Syst.* 12:117–27
89. Flauraud V, Mastrangeli M, Bernasconi GD, Butet J, Alexander DT, et al. 2017. Nanoscale topographical control of capillary assembly of nanoparticles. *Nat. Nanotechnol.* 12:73–80
90. Collet M, Salomon S, Klein NY, Seichepine F, Vieu C, et al. 2015. Large-scale assembly of single nanowires through capillary-assisted dielectrophoresis. *Adv. Mater.* 27:1268–73

Annual Review of Control, Robotics, and Autonomous Systems

Volume 6, 2023

Contents

An Overview of Soft Robotics
Oncay Yasa, Yasunori Toshimitsu, Mike Y. Michelis, Lewis S. Jones, Miriam Filippi, Thomas Buchner, and Robert K. Katzschmann 1

Soft Actuators and Robots Enabled by Additive Manufacturing
Dong Wang, Jinqiang Wang, Zequn Shen, Chengru Jiang, Jiang Zou, Le Dong, Nicholas X. Fang, and Guoying Gu 31

Adaptive Control and Intersections with Reinforcement Learning
Anuradha M. Annaswamy 65

On the Timescales of Embodied Intelligence for Autonomous Adaptive Systems
Fumiya Iida and Fabio Giardina 95

Toward a Theoretical Foundation of Policy Optimization for Learning Control Policies
Bin Hu, Kaiqing Zhang, Na Li, Mehran Mesbahi, Maryam Fazel, and Tamer Başar 123

Sequential Monte Carlo: A Unified Review
Adrian G. Wills and Thomas B. Schön 159

Construction Robotics: From Automation to Collaboration
Stefana Parascho 183

Embodied Communication: How Robots and People Communicate Through Physical Interaction
Aleksandra Kalinowska, Patrick M. Pilarski, and Todd D. Murphey 205

The Many Facets of Information in Networked Estimation and Control
Massimo Franceschetti, Mohammad Javad Khojasteh, and Moe Z. Win 233

Crowd Dynamics: Modeling and Control of Multiagent Systems
Xiaoqian Gong, Michael Herty, Benedetto Piccoli, and Giuseppe Visconti 261

Noise in Biomolecular Systems: Modeling, Analysis, and Control Implications
Corentin Briat and Mustafa Khammash 283

Exploiting Liquid Surface Tension in Microrobotics
Antoine Barbot, Francisco Ortiz, Aude Bolopion, Michaël Gauthier, and Pierre Lambert 313

Spacecraft-Mounted Robotics
Panagiotis Tsiotras, Matthew King-Smith, and Lorenzo Ticozzi 335

Grasp Learning: Models, Methods, and Performance
Robert Platt 363

Control of Multicarrier Energy Systems from Buildings to Networks
Roy S. Smith, Varsha Behrunani, and John Lygeros 391

Control of Low-Inertia Power Systems
Florian Dörfler and Dominic Groß 415

How the CYBATHLON Competition Has Advanced Assistive Technologies
Lukas Jaeger, Roberto de Souza Baptista, Chiara Basla, Patricia Capsi-Morales, Yong Kuk Kim, Shuro Nakajima, Cristina Piazza, Michael Sommerhalder, Luca Tonin, Giacomo Valle, Robert Riener, and Roland Sigrist 447

Into the Robotic Depths: Analysis and Insights from the DARPA Subterranean Challenge
Timothy H. Chung, Viktor Orekhov, and Angela Maio 477

Errata

An online log of corrections to *Annual Review of Control, Robotics, and Autonomous Systems* articles may be found at http://www.annualreviews.org/errata/control